Published in final edited form as:
Pharm Res. 2013 May ; 30(5): 1240–1251. doi:10.1007/s11095-012-0963-6.

Design and Characterization of a Novel Fluorinated Magnetic Resonance Imaging Agent for Functional Analysis of Bile Acid Transporter Activity

Diana Vivian[1], **Kunrong Cheng**[2], **Sandeep Khurana**[2], **Su Xu**[3], **Valerie Whiterock**[4], **Drew Witter**[4], **Kimberley A. Lentz**[4], **Kenneth S. Santone**[4], **Jean-Pierre Raufman**[2], and **James E. Polli**[1,5]

[1]Department of Pharmaceutical Sciences, School of Pharmacy, University of Maryland, Baltimore, Maryland [2]Department of Medicine, School of Medicine, University of Maryland, Baltimore, Maryland [3]Department of Diagnostic Radiology and Nuclear Medicine, School of Medicine, University of Maryland, Baltimore, Maryland [4]Bristol Myers Squibb, Wallingford, Connecticut.

Abstract

Purpose—Our objectives were to synthesize a trifluorinated bile acid that can be used for ^{19}F magnetic resonance imaging (MRI) of bile acid enterohepatic circulation, characterize its *in vitro* transporter affinity, stability, and ^{19}F-MRI signal, and assess its ability to concentrate in the gallbladder of C57BL/6 mice.

Methods—Target compound CA-lys-TFA was synthesized and tested for affinity toward the apical sodium dependent bile acid transporter (hASBT) and the Na+/taurocholate cotransporting polypeptide (hNTCP). In a pilot study, fasted mice were gavaged with vehicle control, 150 mg/kg or 300 mg/kg CA-lys-TFA. CA-lys-TFA in gallbladder, liver and plasma at t=5 h was quantified. Additionally, a 24-h time course (24 mice across eight time points) was studied using 50 mg/kg CA-lys-TFA.

Results—CA-lys-TFA was a potent substrate of hASBT (Kt=39.4 μM, normalized Vmax=0.853) and hNTCP (Kt=8.99 μM, normalized Vmax=0.281). ^{19}F MRI phantom imaging showed linear signal-concentration dependence. *In vivo* studies showed that rapid accumulation of CA-lys-TFA in the gallbladder was maximal within 4-7 h.

Conclusion—These findings suggest that CA-lys-TFA, a fluorinated non-radioactive bile acid analogue, has potential for use in MRI to measure *in vivo* bile acid transport and diagnose bile acid malabsorption and other conditions associated with impaired bile acid transport.

Keywords

Bile acid transport; fluorine MRI; apical sodium-dependent bile acid transporter; Na+/taurocholate cotransporting polypeptide; enterohepatic circulation

[5]To whom correspondence should be addressed: James Polli (University of Maryland School of Pharmacy, 20 Penn Street, HSF2 room 623, Baltimore, MD 21201 USA Tel: 410-706-8292; Fax: 410-706-0517; jpolli@rx.umaryland.edu).

INTRODUCTION

Bile acids are synthesized in the liver as by-products of cholesterol metabolism, conjugated with glycine or taurine, and secreted into bile. In humans, mice and other species containing a gallbladder, bile is stored in that organ until release into the small intestine following a meal, where bile acids aid in lipid digestion. Bile acids are passively absorbed throughout the small intestine. However, in the terminal ileum, bile acids are actively absorbed by hASBT (*SLC10A2*, the human apical sodium dependent bile acid transporter) into intestinal epithelial cells and then effluxed by the organic solute transporters (OSTα-OSTβ) into the portal circulation, thereby returning to the liver.

hNTCP (*SLC10A1*, the Na+/taurocholate cotransporting polypeptide) and the organic anion transporting peptides (OATPs), located on the hepatocyte basolateral membrane, transport bile acids into hepatocytes. hNTCP accounts for almost all Na+-dependent hepatic uptake of bile acids from the portal circulation (1). Bile acids are subsequently effluxed into bile by the bile salt export pump (BSEP) and the multidrug resistance associated protein 2 (MRP2).

Overall, this enterohepatic circulation of bile acids provides a highly efficient mechanism for their conservation. Whereas the total human bile acid pool of 2-4 g undergoes enterohepatic circulation several times each day, only ~0.5 g/day of bile acids are lost in the stool (2, 3). Bile acid malabsorption (BAM) results in excess fecal bile acids that can cause chronic diarrhea and other colon pathology. BAM can be attributed to genetic mutations in hASBT (4, 5), ileal disease (e.g. Crohn's disease) and surgical resection. Not surprisingly, Asbt-deficient mice have increased levels of fecal bile acids (6). Alternatively, BAM can also result from increased hepatic production of bile acids that overwhelms ASBT transport capacity (7). It is estimated that BAM, which is commonly misdiagnosed as irritable bowel syndrome, is responsible for 30-50% of unexplained chronic diarrhea (8, 9).

In Europe, BAM is commonly diagnosed with a clinical test using ^{75}Se-HCAT, a gamma-emitting ^{75}Se-labeled synthetic bile acid (10). However, this method has important limitations; ^{75}Se-HCAT emits low levels of radiation and is not approved for use in the United States – its use is limited to a few European countries.

Our work is focused on developing ^{19}F MRI as a novel imaging method to diagnose BAM. Unlike ^{18}F which is used in positron emission tomography (PET) imaging, ^{19}F, the sole naturally-occurring, stable fluorine isotope, is neither radioactive nor limited by a short radioactive half-life. ^{19}F MRI imaging is non-invasive and second to only ^{1}H MRI in terms of MRI sensitivity. Unlike ^{1}H MRI, which detects endogenous water signals from the body, ^{19}F MRI benefits from the absence of background interference (i.e. no background ^{19}F in tissues) so it is well suited to image drug molecules containing fluorine atoms (11). Additionally, the ^{19}F MRI signal is directly proportional to the fluorine concentration (12).

Since bile acids accumulate in the gallbladder between meals, as a proof-of-concept we demonstrated previously that a trifluorinated drug, isoflurane, accumulates in the gallbladder. We determined the limit of detection of isoflurane by ^{19}F MRI imaging to be approximately 1 mM, equivalent to 3 mM total fluorine atoms (13). In the present report, our objectives were to synthesize a trifluorinated bile acid; characterize *in vitro* its affinity for bile acid transporters,stability and ^{19}F MRI signal; and measure its ability to concentrate in the murine gallbladder above the ^{19}F MRI limit of detection. The findings detailed in this report indicate that the resulting molecule, CA-lys-TFA, possesses chemical properties that make it a suitable reagent for *in vivo* studies of bile acid transport using ^{19}F MRI.

MATERIALS AND METHODS

Materials

[^{3}H]-taurocholic acid (10 μCi/mM) was obtained from American Radiolabeled Chemicals, Inc. (St. Louis, Missouri). Taurocholate, cholic acid, trifluoroacetyl L-lysine, rat liver S9 fraction, rat plasma, and choloylglycine hydrolase from *Clostridium perfringens* were purchased from Sigma Aldrich (St. Louis, Missouri). Geneticin, trypsin, Dulbecco's modified Eagle medium (DMEM), and fetal bovine serum (FBS) were purchased from Invitrogen (Rockville, Maryland). All other reagents and chemicals were of the highest purity commercially available.

Methods

Synthesis of fluorinated bile acid—The synthesis of cholic acid-trifluoroacetyl lysine (CA-lys-TFA) is shown in Figure 1. Two g cholic acid (4.89 mmol) was stirred in 15 mL dimethyl formamide (DMF) at room temperature (RT). To this was added 1 eq. (0.68 mL) triethylamine (TEA) and 1 eq. (1.86 g) O-benztriazol-1-yloxytris-1,1,3,3 tetra methyl uranium hexaflourophosphate (HBTU). After 15 min, 1 eq. (0.78 g) hydroxybenzotriazole (HOBt) was added and the mixture was stirred for 4 h. The resulting product was extracted with 60 mL ethyl acetate (EtOAc) and washed with 30 mL water (3x), then with 20 mL brine (2x). The EtOAc layer was dried with sodium sulfate, filtered and solvent was removed by evaporation. An appropriate MS peak of [M + 1] 526.4 was shown and the activated benzotriazole (OBt) ester of cholic acid was used without further purification.

One eq. (1.8 g) trifluoroacetyl L-lysine was added to 4 g activated cholic acid OBt ester and stirred in DMF at RT for 16 h. The resulting product was extracted with 80 mL EtOAc, washed with 30 mL water (3x), 20 mL 1 M HCl (3x), 30 mL water (3x), and extracted with 30 mL 1 M NaOH (1x). This aqueous extract was subsequently acidified to pH 1 using concentrated HCl and extracted into 80 mL EtOAc, then washed with 30 mL water (3x), 30 mL brine (3x), and the organic layer was dried using sodium sulfate. The resulting solution was filtered and evaporated to remove EtOAc. Compound purity was determined by analysis on a Waters HPLC system consisting of a Waters 1525 binary HPLC pump, Waters 486 tunable absorbance detector, and a Waters 717 plus autosampler (Waters Corporation, Milford, MA). A Restek column (ultra phenyl, 5 μm, 250 × 4.6 mm) was used (Restek Corporation, Bellefonte, PA). Two orthogonal chromatographic methods were employed: one with methanol-[20 mM ammoniun formate, 0.5% formic acid, 0.2% triethylamine (pH 3)] 67:33 v/v (14) and the second with 50% ACN, 50% water, 0.1% formic acid. The compound was eluted at a flow rate of 1.0 mL/min and detected at 218 nm. The methods were linear over the range of 25 to 200 μM (method one r^2=0.998, method two r^2= 0.961). NMR was acquired using Varian VNMRS 400 MHz. The target compound IUPAC name is (S)-6-(2,2,2-trifluoroacetamido)-2-((R)-4-((3R,5S,7R,8R,9S,10S,12S,13R,14S,17R)-3,7,12-trihydroxy-10,13-dimethylhexadecahydro-1H-cyclopenta[α]phenanthren-17-yl)pentanamido)hexanoic acid.

Cell Culture—Stably transfected hASBT-MDCK cells were cultured at 37°C, 90% humidity, 5% CO_2, and fed every two days, as previously described (15). Media consisted of DMEM fortified with 10% FBS, 50 units/mL penicillin and 50 μg/mL streptomycin. Geneticin (1 mg/ml) was added to maintain selection pressure. Cells were passaged after reaching 90% confluency (approximately every 4 days).

Stably transfected hNTCP-HEK cells were cultured as previously described (16). Briefly, cells were grown at 37°C, 90% humidity, 5% CO_2, and fed every two days. Media consisted of DMEM fortified with 10% FBS, 1% nonessential amino acids, 50 units/mL penicillin,

and 50 μg/mL streptomycin. Geneticin (1 mg/ml) was added to maintain selection pressure. Cells were passaged after reaching 90% confluency (approximately every 4 days).

Uptake of CA-lys-TFA by hASBT and hNTCP—hASBT-MDCK cells were seeded at a density of 1.5 million cells/well in 12-well plates (3.8 cm^2). On day-four after seeding and 15 h prior to uptake studies, cells were induced with 10 mM sodium butyrate. hNTCP-HEK cells were seeded at a density of 0.6 million cells/well in 24-well plates (2 cm^2), and were exposed to donor solution 2 days after seeding. Donor solution consisted of Hank's balanced salt solution [HBSS; Sigma Aldrich (St. Louis, Missouri)] or sodium-free buffer (SFB) and 0-200 μM CA-lys-TFA. SFB replaced NaCl with 137 mM tetraethylammonium chloride and was used to determine sodium-independent passive permeability. Cells were washed three times with either HBSS or SFB (consistent with donor) and exposed to donor solution.

After 10 min incubation on an orbital shaker at 37°C for hASBT-MDCK cells and 5 min for hNTCP-HEK cells, wells were rinsed three times with cold SFB. Ten and 5 min represent periods of linear bile acid uptake based on previous observations for these stably transfected cell lines (15, 16). Cells were lysed using 300 μL ACN for MDCK cells as previously described (17) and 150 μL ACN for HEK cells and left to evaporate at RT for 3 h. Compound was then extracted with 1:1 ACN:water. Extracts were stored at -80°C in silanized centrifuge tubes until analysis. Taurocholate Vmax was estimated using a saturating concentration of 200 μM on each study occasion. Taurocholate donor solutions were spiked with 0.5 μCi/mL [^{3}H] taurocholate. Lysates were counted for radioactivity using a LS6500 liquid scintillation counter (Beckmann Instruments, Inc., Fullerton, California).

CA-lys-TFA Km was estimated using regression by WinNonlin [Pharsight; St. Louis, Missouri] of a modified Michaelis-Menten equation (eqn. 1), as previously described (18).

$$V = \frac{P_{ABL} \cdot \left(\frac{V_{max}}{K_m + S} + P_p\right)}{P_{ABL} + \frac{V_{max}}{K_m + S} + P_p} \cdot S \quad \text{(eqn. 1)}$$

where V is substrate flux, P_{ABL} is aqueous boundary layer permeability, P_p is passive permeability, and S is substrate concentration. P_{ABL} was set to 1.5×10^{-4} cm/s (19).

CA-lys-TFA concentration was determined by liquid chromatography/mass spectrometry (LC/MS) on a Waters Acquity UPLC system with triple quadrupole detector (Waters Corporation, Milford, MA). The column used was a Waters Acquity UPLC Ethylene Bridged Hybrid C8 1.7 μm 2.1x50 mm. The flow rate was 0.4 mL/min with a gradient as follows (expressed at % ACN in water, all mobile phases including 0.1% formic acid): 50% from 0 to 1 min, then increased to 95% until 2.5 min, then decreased to 50% at 3 min and held at 50% until 4 min. Injection volume was 10 μL. Dwell time was 0.010 seconds and cone voltage was 78V. Negative ion electrospray ionization mode was used along with a single ionization reaction method for 632.28 Da. The method was linear over the range of 5 to 2000 nM (r^2 = 0.9997).

CA-lys-TFA Solubility in Buffer—Ten mg compound in silanized centrifuge tubes was introduced to 200 μL phosphate buffer at pH 6.8 and pH 8 (n=3 for each). Vials of suspension were shaken at RT overnight. After shaking, tubes were centrifuged at 10,000 g for 15 min. Supernatant was removed and diluted 1000x with ACN before analysis by LC/MS as described above.

***In Vitro* Stability of CA-lys-TFA—**Stability of 5 μM conjugate was evaluated in Caco-2 homogenates to simulate the intestinal epithelia, rat plasma, rat liver s9 fraction, simulated

intestinal fluid with pancreatic enzymes (SIF), 1 M HCl to represent stomach conditions, and choloylglycine hydrolase (CGH) to simulate conditions in the colon. CGH is a bile acid-deconjugating bacterial enzyme present in small amounts in the terminal ileum and higher amounts in the colon. Stability was also evaluated using DPBS at pH 7.4, HBSS at pH 6.8, and hASBT-MDCK and hNTCP-HEK homogenates to ensure stability through *in vitro* uptake experiments,

Caco-2 cells were cultured as previously described (20). Briefly, cells were grown in 225 cm^2 flasks at 37°C and 5% CO_2 for 21 days. Cells were cultured in DMEM fortified with 1% nonessential amino acids, 10% FBS, 50 units/mL penicillin, and 50 μg/mL streptomycin. Cells were washed three times with Dulbecco's phosphate buffered saline (DPBS), scraped over ice and reconstituted in 10 mL DPBS. Reconstituted cells were stored overnight at -80°C, thawed over ice, and homogenized using a sonic dismembrator (model F60; Fisher Scientific, Pittsburgh, Pennsylvania) at 5 to 6 W (RMS). Homogenate was centrifuged at 10,000 g for 15 min at 4°C. Protein concentration of the supernatant was measured using the Bio-Rad assay (Bio-Rad Laboratories, Inc, Hercules, California). Aliquots of 1 mL Caco-2 homogenate containing 0.485 mg/mL protein were stored at -80°C until use. hASBT-MDCK and hNTCP-HEK cells were cultured as in uptake studies and were homogenized in the same manner as Caco-2 cells.

Rat plasma was used with and without addition of 1 mM phenylmethylsulfonyl fluoride (PMSF), a protease inhibitor. Rat Liver S9 Fraction was used at 1 mg/mL in DPBS with and without addition of 1 mM NADPH. SIF with pancreatic enzymes was prepared according to the USP28 method modified previously (21). Solutions consisted of 0.2 M NaOH, 6.8 g/L monobasic potassium phosphate, and 10 g/L pancreatin, adjusted to pH 7.5. For stability studies, 1 mL solutions were incubated at 37°C before initiating the study by adding 5 μM CA-lys-TFA.

CGH from *Clostridium perfringens* solution was prepared as previously described (22). Briefly, 10 mM mercaptoethanol, 1 mM ethylenediaminetetraacetic acid (EDTA), and 2 mM CA-lys-TFA were added to 5 mM sodium acetate buffer at pH 5.6. After incubation at 37°C, the study was started by adding 15 U CGH.

For most stability studies, 100 μL samples were taken at time 0, 15 min, 30 min, 1 h, 2 h, 3 h, and 4 h (DPBS and HBSS at 0, 1, 2, and 3 h), quenched with 400 μL 4°C ACN, centrifuged at 10,000 g for 15 min, and stored at -80°C until analysis by LC/MS as described above. Stability of CA-lys-TFA was evaluated in hASBT-MDCK homogenate and hNTCP-HEK homogenate after 10 min and 5 min, respectively, to correspond with the time period of uptake studies.

***In Vitro* ^{19}F MRI of CA-lys-TFA—**Both ^{1}H and ^{19}F MRI analysis of CA-lys-TFA samples were performed on a Bruker BioSpec 70/30USR Avance III 7T horizontal bore MR scanner (Bruker Biospin MRI GmbH, Germany), equipped with a BGA12S gradient system and interfaced to a Bruker Paravision 5.1 console. A Bruker 30-mm ^{19}F/^{1}H dual-tuned surface coil was used to transmit and receive radiofrequency (RF) signals at 300.28 MHz for ^{1}H and 282.55 MHz for ^{19}F nuclei. All MRI experiments were performed at RT.

2-mL clear glass vials (National Scientific, Rockwood, Tennessee) were used for imaging and CA-lys-TFA was dissolved in methanol. Two vials were bundled together with paper tape for imaging. The 30 mM CA-lys-TFA sample-vial was used as a standard in the acquisition of 0, 10 and 20 mM CA-lys-TFA samples whose ^{19}F MRI signal intensities were normalized against the 30 mM sample. Therefore, samples were grouped in the following way: 0 mM/30 mM, 10 mM/30 mM, and 20 mM/30 mM.

After the two-vial sample was centered in the magnet, the radio frequency coil was tuned and matched to the ^{1}H signal. A three-slice (axial, mid-sagittal, and coronal) scout ^{1}H MRI using fast low angle shot (FLASH) sequence (23, 24) was obtained to localize the volume of interest. A single slice ^{1}H MR image was acquired using FLASH sequence in the cross view of the sample with repetition time = 100 ms, echo time = 7.9 ms, Flip angle = 30^{0}, field of view = 6 × 6 cm^{2}, slice thickness = 4 mm, matrix size = 512 × 512, in-plane resolution = 0.117 × 0.117 mm^{2}, and number of averages = 1. Total acquisition time was not more than 1 min.

After the radio frequency coil was tuned and matched to the ^{1}H signal, low resolution ^{19}F images were acquired using the FLASH sequence in the same region of the ^{1}H MRI with repetition time = 100 ms, echo time = 6 ms, matrix size = 64 × 64, in-plane resolution = 0.938 × 0.938 mm^{2}. The rest of the parameters were the same as ^{1}H MRI. Acquisition time was varied with no more than 7 min for 20 mM/30 mM two-vial sample (number of average (na) = 64), 28 min for 10 mM/30 mM two-vial sample (na = 256), and 56 min for 1 mM/30 mM two-vial sample (na = 512), and 7 min for 0 mM/30 mM two-vial sample (na=64).

In Vivo Disposition and Characterization of CA-lys-TFA Transport: Pilot Study—All animal studies were conducted in accordance with the *Guide for the Care and Use of Laboratory Animals* prepared by the U.S. National Academy of Sciences (25). Mouse studies were approved by both the Institutional Animal Care and Use Committee at the University of Maryland School of Medicine and the Research and Development Committee at the VA Maryland Health Care System. C57BL/6 mice were obtained from Jackson Labs, Bar Harbor, Maine and housed under identical conditions in a pathogen-free environment with a 12:12-hour light/dark cycle and free access to standard mouse chow and water for one week prior to treatment. Eight male C57BL/6J mice (13 weeks old, 25.7 g average weight) were used for *in vivo* studies. Mice were fasted overnight. At the time of dosing, 2 mice (mice 1 and 2) were used as control and were orally gavaged with 8.33 μL vehicle (1:1 polyethylene glycol(PEG)400:water) per g body weight. Three mice (mice 3, 4 and 5) were gavaged with 150 mg/kg CA-lys-TFA in vehicle and three mice (mice 6, 7 and 8) with 300 mg/kg CA-lys-TFA in vehicle. Five h post dosing, mice were anesthetized with ketamine/xylazine and gallbladder, liver and blood were collected, along with stomach and small intestine. Gallbladder and blood samples were used exclusively for CA-lys-TFA quantification. Liver was used for both CA-lys-TFA quantification and histologic analysis. Stomach and small intestine were exclusively used for histologic analysis.

Portions of liver, stomach, and small intestine were fixed in formalin for 3 days, then transferred to 70% ethanol and stored at -20°C until cutting and staining. Whole gallbladder and portions of liver were kept on ice, homogenized using a Duall size 21 glass tissue homogenizer and extracted with 75% ACN in water. Blood samples were collected in heparinized tubes then centrifuged to obtain plasma. Plasma proteins were precipitated with 4 parts ACN and centrifuged at 10,000 g for 10 min.

In Vivo Pharmacokinetics and Disposition of CA-lys-TFA—Favorable results from the pilot study motivated a pharmacokinetic evaluation from 0-24 h, using a lower oral dose of 50 mg/kg. Mouse studies were approved by the Institutional Animal Care and Use Committee at Bristol-Myers Squibb. C57BL/6 mice were obtained from Charles River Laboratories International, Inc., Wilmington, Massachusetts and housed in a pathogen-free environment with a 12:12-hour light/dark cycle, with free access to standard mouse chow and water for one week prior to treatment. Twenty-four male C57BL/6J mice (6-8 weeks old, 23.9 g average weight) were used for *in vivo* studies. Mice were fasted overnight and allowed access to food at 4 h after dosing. At the time of dosing, mice were orally gavaged with 50 mg/kg CA-lys-TFA via 10 μL vehicle (1:1 polyethylene glycol(PEG)400:water) per

g body weight. For each 0.5, 1, 2, 3, 5, 7 and 24 h post dosing, three mice were euthanatized with CO_2 and gallbladder, liver and blood were collected. For 0 h, the three mice were not dosed with CA-lys-TFA, but euthanatized with CO_2 and gallbladder, liver and blood were collected. Hence, 24 mice across eight time points were employed via destructive sampling, with N=3 per time point. Gallbladder, liver, and blood samples were used for CA-lys-TFA quantification.

Livers were homogenized and gallbladders were sonicated and extracted with phosphate buffer. Plasma proteins were precipitated with four parts ACN using a Phenomenex Strata Protein Precipitation Plate (Phenomenex, Torrance, California). Concentrations of CA-lys-TFA in gallbladder and liver were calculated assuming a tissue density of 1 g/mL.

CA-lys-TFA concentration was determined by liquid chromatography/mass spectrometry (LC/MS/MS) on an Agilent 1200 series UPLC system (Agilent Technologies, Santa Clara, California) and API 4000 Qtrap (AB SCIEX, Framingham, Massachusetts). Detection of CA-lys-TFA was performed using selected reaction monitoring. The column used was a Waters Acquity UPLC HSS T3 1.3 um 50 × 2.1 mm. The column temperature was 60°C and the flow rate was 0.6 mL/min with a gradient as follows (expressed at % ACN in water, all mobile phases including 0.1% formic acid): 5% from 0 to 0.2 min, then increased to 95% until 1.1 min, held at 95% until 1.4 min, then decreased to 5% at 1.5 min and held at 50% until 2 min. Dwell time was 0.050 seconds. The ion transition 633.5 → 579.6 was monitored from positive ion electrospray ionization. The method was linear over the range of 1.22 to 10,000 nM ($r^2 = 0.9937$).

Pharmacokinetic Analysis—Pharmacokinetic parameters were obtained by non-compartmental analysis of mean concentration versus time data (Thermo Kinetica software, Version 5.0; Thermo Fisher Scientific Corporation, Waltham, Massachusetts) in plasma, liver, and gallbladder (n=3 mice per timepoint). The peak concentration (Cmax) and time for Cmax (Tmax) were recorded directly from mean experimental observations. The area under the curve from time zero to the last sampling time [AUC(0-T)] was calculated using a combination of linear and log trapezoidal summations.

Statistical Analysis—Student's paired *t*-test was used to evaluate stability data. Student's *t*-test was also used to evaluate effects of different doses of CA-lys-TFA on its concentration in gallbladder, liver and plasma. A p-value of 0.05 was used as the cut-off for statistical significance. In figures and reported values, error bars denote standard error of the mean throughout.

RESULTS

Synthesis of fluorinated bile acid

MS showed the appropriate peak at [M – 1] 631.5 Da and [M + 1] 633.4 Da. MS confirmed that cholic acid was not present in the final product. HPLC method 1 R_T =3.8 min, method 2 R_T = 8.8 min (purity 97.5%). ^{13}C NMR (DMSO-d6): δ 12.77, 17.56, 23.05, 23.16, 23.23, 26.64, 27.73, 28.23, 28.98, 30.83, 30.97, 32.09, 32.63, 34.82, 35.32, 35.57, 35.73, 39.60, 39.95, 40.20, 41.79, 41.95, 46.15, 46.59, 51.98, 66.66, 70.85, 71.44, 118.77, 156.38, 173.26, 174.28 (Peaks 39.60, 39.95, and 40.20 were obscured by DMSO-d6 solvent and were obtained from HMBC).

Uptake by hASBT and hNTCP

Figures 2 and 3 illustrate the uptake of CA-lys-TFA by hASBT and hNTCP, respectively. CA-lys-TFA was a potent substrate for both hASBT and hNTCP *in vitro*. In the absence of

sodium, less CA-lys-TFA was taken up into hASBT-expressing and hNTCP-expressing cells, reflecting bile acid transporter-mediated uptake of CA-lys-TFA.

For hASBT, the Km was 39.4 ± 23.8 μM, which is a few-fold less potent that taurocholate's Km of 4.39 μM, yet still potent (18). Vmax was 0.148(±0.033) $\times 10^{-3}$ nmol/cm^2/s. NormVmax (i.e. Vmax normalized against taurocholate Vmax on the same occasion) was 0.853 ± 0.197, indicating that Vmax for CA-lys-TFA was 85% of that for the native substrate taurocholate. Passive permeability was a low 0.276(±0.066) $\times 10^{-6}$ cm/s, which was even less than that of taurocholate (18).

For hNTCP, the Km was 8.99 ± 2.79 μM, which is comparable to taurocholate's Km of 5.31 μM (26). Vmax was 0.747(±0.048) $\times 10^{-3}$ nmol/cm^2/s. NormVmax was 0.281 ± 0.052, indicating Vmax for CA-lys-TFA was about one-fourth that for taurocholate. Passive permeability was 0.208(±0.174) $\times 10^{-6}$ cm/s.

Solubility in Buffer

CA-lys-TFA solubility in phosphate buffer at pH 6.8 was 17.2 ± 1.96 mM. At pH 8, solubility increased to 36.0 ± 2.85 mM, in agreement with the weakly acidic nature of CA-lys-TFA. Solubility at each pH exceeded the 3 mM fluorine atom requirement (i.e. 1 mM trifluorinated compound) for the ^{19}F-MR imaging limit of quantification.

In Vitro Stability

In Figure 4, incubation of 5 μM CA-lys-TFA in Caco-2 homogenate, rat plasma, rat liver s9 fraction, SIF, 1 M HCl, DPBS at pH 7.4, and HBSS at pH 6.8 showed no significant compound loss at the longest time tested ($p<0.05$; Student's paired *t*-test). Additionally, incubation of 5 μM CA-lys-TFA in hASBT-MDCK homogenate and hNTCP-HEK homogenate for 10 min and 5 min, respectively, showed no significant compound loss. CA-lys-TFA stability in hNTCP-HEK homogenate (n=7) was 97.2 (± 2.4)% and in hASBT-MDCK homogenate (n=5) was 101.9 (± 6.3)%.

Stability of CA-lys-TFA in CGH showed significant degradation (Figure 5 panel A), but at a much slower rate than the deconjugation of the natural bile acid conjugate taurocholate (Figure 5 panel B). Panel A and B show the disappearance of CA-lys-TFA and taurocholate, respectively, as well the appearance of cholic acid. CA-lys-TFA degraded to less than 10% of the original concentration in 3 h (5.87 ± 0.31%). In contrast, taurocholate had already degraded to less than 10% (2.36 ± 0.48%) within 1 h. These findings suggest improved stability of the amide bond linking trifluoroacetyl lysine to cholic acid compared to the natural amino acid conjugate.

In Vitro ^{19}F MRI of CA-lys-TFA

Figure 6 (panel A) shows ^{19}F MRI imaging of 0, 10 and 20 mM CA-lys-TFA phantoms, as well as 30 mM CA-lys-TFA phantoms. This panel was composed of the three acquisitions described in Materials and Methods, where the 0, 10 or 20 mM CA-lys-TFA phantoms were measured and normalized against a 30 mM CA-lys-TFA phantom. In Figure 6 (panel B), ^{19}F MRI *in vitro* testing showed linear dependence of signal strength on CA-lys-TFA concentration (r^2=0.993). As described above, the CA-lys-TFA concentration in mouse gallbladder was 31.9 mM. Hence, the ability to detect a ^{19}F MRI signal strength versus CA-lys-TFA concentration relationship between 0-30 mM supports the merit of further investigation of *in vivo* ^{19}F MRI using this novel probe. Moreover, results from these *in vitro* phantom studies suggest that *in vivo* acquisition times of one hour or less may be feasible.

Oral Disposition Characterization of CA-lys-TFA: Pilot Study

As expected, CA-lys-TFA was not detected in the gallbladder, liver or plasma of control mice (Table I) by LC/MS analysis, as these animals were not dosed with CA-lys-TFA.

LC/MS analysis of tissues obtained from CA-lys-TFA-treated mice showed robust accumulation of CA-lys-TFA in the gallbladder at 5 h. Concentrations of CA-lys-TFA in gallbladder and liver were obtained by assuming an organ density of 1 g/mL. In Table I, CA-lys-TFA concentration in the gallbladder of mice dosed at 150 mg/kg was 27.0 ± 2.4 mM. The gallbladder concentration with the 300 mg/kg dose was 36.8 ± 8.8 mM. Gallbladder concentrations of CA-lys-TFA were not significantly different between the two dose levels (p=0.35; Student's *t*-test). The CA-lys-TFA concentration in the gallbladder from each dosed mouse exceeded the 3 mM fluorine atom requirement (i.e. 1 mM trifluorinated compound) for imaging limit of quantification. Across both dose levels, the average CA-lys-TFA concentration in the gallbladder was 31.9 ± 4.6 mM (95% confidence interval, 20.0–43.8 mM).

The percent dose that accumulated in the gallbladder at 5 h was 11.0 ± 1.7% for the 150 mg/kg dose and 5.33 ± 1.98% for the 300 mg/kg dose. Across both dose levels, the percent accummulation in gallbladder was 8.18 ± 1.73% (95% confidence interval, 3.72-12.64%).

CA-lys-TFA concentrations in the liver were much lower than in the gallbladder (Table I). CA-lys-TFA liver concentration from the 150 mg/kg dose was 0.0788 ± 0.0351 mM, and 0.0571 ± 0.0104 mM from the 300mg/kg dose. CA-lys-TFA concentrations were not significantly different between the two dose levels (p=0.58; Student's *t*-test). CA-lys-TFA concentration in the liver of each mouse was below the 3 mM fluorine atom requirement (i.e. 1 mM trifluorinated compound) for imaging limit of quantification. These measurements reflect favorable targeting of CA-lys-TFA to the gallbladder. Across both dose levels, the average CA-lys-TFA concentration in liver was 0.0680 ± 0.0171 mM (95% confidence interval 0.0240 – 0.1119 mM).

Plasma concentrations of CA-lys-TFA were significantly less than those in the gallbladder (Table I). Plasma concentrations with the 150 and 300 mg/kg doses were 0.444 ± 0.170 μM and 0.418 ± 0.045 μM, respectively. Like those in the liver, these concentrations were lower than the limit of quantification for ^{19}F MRI imaging and reflect favorable targeting of CA-lys-TFA to the gallbladder.

Histology

Stomach and liver tissues of mice in all treatment groups appeared grossly normal by visual inspection and microscopic examination of hematoxylin and eosin (H&E)-stained sections. In Figure 7, H&E analysis of small intestine from two of three mice treated with the 300 mg/kg dose (i.e. higher dose) showed mild loss of nuclei and cytoplasmic vacuolization at the tips of the intestinal villi. These changes were not seen in any of the three mice treated with 150 mg/kg CA-lys-TFA.

Oral Pharmacokinetics and Disposition of CA-lys-TFA

Figure 8 shows the mean concentration of CA-lys-TFA in mouse gallbladder, liver, and plasma at time 0, 0.5, 1, 2, 3, 5, 7 and 24 h after oral administration of 50 mg/kg CA-lys-TFA. In Panel A, LC/MS/MS analysis of tissues obtained from CA-lys-TFA-treated mice showed robust accumulation of CA-lys-TFA in the gallbladder, consistent with pilot study results. Gallbladder concentrations observed were several-fold higher than in the liver and plasma. Panel B shows an expanded view of the lower concentrations of CA-lys-TFA in the liver and plasma.

In Table II, the non-compartmental pharmacokinetic parameters obtained from CA-lys-TFA concentrations in tissue are presented. The gallbladder Cmax was 11.1 ± 2.4 mM, and occurred at seven hours after dosing. Liver Cmax was 16.3 ± 3.1 μM at t = 1h, and plasma Cmax was 24.8 ± 19.6 μM at t = 5 h. The gallbladder Cmax was over 13,000 times higher than that of the liver and over 1,000 times higher than the plasma Cmax, showing successful targeting.

Measured concentrations from the 50 mg/kg study were generally lower than those from the higher dose pilot studies, which employed 150 mg/kg and 300 mg/kg and only sampled at t=5 h. The gallbladder concentration at t=5 h from 50 mg/kg was 5.20 mM, which was about 5- to 7-fold less than that from each pilot study. The liver concentration at t=5 h from 50 mg/kg was 0.0127 mM, which was also about 5- to 7-fold less than that from each pilot study. Individual plasma concentrations at t=5 h from 50 mg/kg were 0.480, 10.3 and 63.6 μM and tended to be higher than those observed from the pilot studies.

DISCUSSION

Need for a novel test to detect impaired bile acid transport and BAM

Bile acids are amongst the most “handled” compounds in the body, reflecting their important roles in lipid digestion and the regulation of key physiological processes such as energy balance (27), glucose metabolism (28), bile acid synthesis (29) and cholesterol metabolism (30). Despite the importance of the enterohepatic circulation of bile acids and drugs, imaging tools are currently not available to “see” this process in living animals. Laboratory methods to measure enterohepatic circulation of bile acids, including sampling mesenteric venous blood and canulating the gallbladder, are both invasive and impractical for use in clinical research or practice. A non-invasive tool to measure bile acid transport *in vivo* would be very useful.

There is a paucity of clinical tests to diagnose BAM. ^{75}Se-HCAT imaging, available in some European countries, involves exposure to small doses of radiation and is not available for use in the United States. Other diagnostic methods, including stool collection for measurement of bile acid concentration or the administration of ^{14}C-taurocholate and measurement in stool (32), are expensive, time consuming and cumbersome. As a surrogate marker of bile acid formation, 7α-hydroxy-4-cholesten-3-one can be measured in serum and has been proposed as a test to identify BAM. However, the compound is relatively unstable and measurement is complex (33). Lastly, blood concentrations of fibroblast growth factor 19 (FGF19) have been proposed as a diagnostic test for BAM; FGF19 concentrations are inversely related to 7α-hydroxy-4-cholesten-3-one levels (34). However, FGF19 levels vary throughout the day and its measurement has not yet been validated as a diagnostic tool.

Thus, although it is infrequently used in clinical practice, a ‘therapeutic trial’ of administering bile acid sequestrants, such as cholestyramine, remains the least expensive, easiest and safest method to diagnose BAM (35). However, bile acid sequestrants are not FDA-approved for this indication, require differing doses across patients, have unfavorable characteristics (e.g. bad taste, reduced bioavailability of co-administered drugs) which commonly result in non-compliance and their use has a high false-negative rate for diagnosing BAM (36). Since BAM is common and requires lifelong treatment, a more definitive, cost-effective, safe and convenient method of diagnosis is needed.

In addition to potentially assisting in the diagnosis of BAM, the development of ^{19}F-bile acid MRI has great potential to translate *in vitro* inhibition/substrate studies from cell culture models to *in vivo* interaction studies. Drug interactions with bile acid transporters have the potential to inhibit bile acid uptake (37). A future goal of our work is to non-invasively

assess *in vivo* inhibition of bile acid transporters by using ^{19}F MRI to measure reduced uptake of CA-lys-TFA in the gallbladder.

Design of CA-lys-TFA

The primary motivation for the work described herein was to develop a non-invasive, non-radioactive method to detect impaired bile acid transport *in vivo* by using ^{19}F MRI imaging of a trifluorinated bile acid compound. Cholic acid was selected due to its high potency for uptake by hASBT, its relatively high aqueous solubility and its relatively low binding to plasma proteins. Compared to other major primary and secondary bile acids, cholic acid has a high aqueous solubility because it possesses three steroidal hydroxyl groups. Its octanol/water partition coefficient is 3.7 compared with chenodeoxycholic acid's partition coefficient of 23.3 (38). ^{19}F-MRI requires the imaging agent to be in solution, and we already calculated the limit of detection of a trifluorinated compound to be approximately 1 mM (13). Additionally, higher aqueous solubility reduces the passive permeability of the compound, allowing for a more specific analysis of active transporter function in enterohepatic circulation. Cholic acid has low plasma protein binding compared with other bile acids, with only 50.2% binding to plasma proteins, versus 96.2% for chenodeoxycholic acid (38). Protein binding results in very short T2 relaxation values, thereby masking fluorine signals (39), thus low protein binding is advantageous.

In designing CA-lys-TFA, wherein trifluoroacetyl lysine is conjugated with cholic acid, trifluoroacetyl lysine was chosen as the fluorine-containing moiety since it affords three equivalent fluorine atoms with low molecular weight. Fluorine MRI signal is proportional to the number of equivalent fluorine atoms present on a molecule (12), thus we sought three equivalent fluorines. The lysine moiety in trifluoroacetyl lysine also allowed the formation of an amide bond with cholic acid, while conserving the negative charge that promotes hASBT uptake (40). The molecular weight of CA-lys-TFA, 632.7 Da, compares favorably with that of cholic acid, 408.6 Da. A substantial portion of the difference in molecular weight (57.0 Da) is accounted for by the three fluorines (25.4 percent).

Once synthesized and purified, CA-lys-TFA was tested against hNTCP and hASBT for inhibitor and substrate potency. CA-lys-TFA was a potent inhibitor and substrate for both transporters. *In vitro* solubility and stability in multiple environments, measured using LC/MS, revealed the new compound to be stable for 3 or 4 h under all conditions, except for CGH treatment. Although CGH catalyzed CA-lys-TFA hydrolysis, deconjugation with CGH was slower than that observed with taurocholate.

In a pilot disposition study, mice were orally gavaged with three doses of CA-lys-TFA (0, 150, and 300 mg/kg) to determine *in vivo* disposition at t =5 h. LC/MS concentration data showed collection of the test agent in the gallbladder, the proposed site of imaging, and much lower concentrations in liver and plasma. Microscopic examination of H&E-stained sections showed no differences between liver and stomach in vehicle-treated mice versus mice dosed at 150 and 300 mg/kg. However, examination of small intestine sections showed minimal damage to small intestinal villi in two animals treated with the 300 mg/kg dose, which was not observed in three mice treated with the 150 mg/kg dose. After the successful pilot study, a pharmacokinetic profile of CA-lys-TFA in mice was obtained using a lower 50 mg/kg dose. LC/MS/MS data for this study confirmed accumulation of CA-lys-TFA in the gallbladder well above the ^{19}F MRI limit of detection, Finally, *in vitro* MRI imaging showed the ^{19}F signal to be directly proportional to CA-lys-TFA concentration.

CONCLUSION

Our objectives were to synthesize a trifluorinated bile acid, characterize its *in vitro* transporter affinity, stability, and ^{19}F MRI signal, and assess its ability to concentrate in the gallbladder above the ^{19}F MRI limit of quantification. CA-lys-TFA was successfully synthesized and found to exhibit favorable properties in terms of affinity for hASBT and hNTCP, stability and ^{19}F MRI signal. CA-lys-TFA concentrated in the mouse gallbladder, with histological examinations showing no damage to small intestine, stomach and liver at a dose of 150 mg/kg dose. The current work indicates that CA-lys-TFA shows favorable characteristics for use in diagnosing *in vivo* inhibition of bile acid uptake and warrants additional study. In future work, we plan to explore the pharmacokinetic profile of CA-lys-TFA *in vivo* in concert with live animal ^{19}F MRI imaging.

Acknowledgments

We acknowledge Dr. Kellie Hom for NMR help, Dr. Cinthia Drachenberg for histology analysis, and Dr. Werner Weitschies for donation of stably transfected hNTCP-HEK cells.

This work was supported by the National Institutes of Health [NIDDK T32 DK067872 Research Training in Gastroenterology; R21 DK093406 and DK67530].

ABBREVIATIONS

MRI	magnetic resonance imaging
MFBA	multifluorinated bile acid
hASBT	the human apical sodium dependent bile acid transporter
hNTCP	the Na+/taurocholate cotransporting polypeptide
BAM	bile acid malabsorption
IBS	irritable bowel syndrome
PET	positron emission tomography
DMEM	Dulbecco's modified Eagle medium
FBS	fetal bovine serum
CA-lys-TFA	cholic acid-trifluoroacetyl lysine
DMF	dimethyl formamide
RT	room temperature
TEA	triethylamine
HBTU	O-benztriazol-1-yloxytris-1,1,3,3 tetra methyl uranium hexafluorophosphate
HOBt	hydroxybenzotriazole
EtOAc	ethyl acetate
MDCK	Madin-Darby canine kidney
HEK	human embryonic kidney
HBSS	Hank's balanced salt solution
SFB	sodium-free buffer
V	substrate flux

P_{ABL}	aqueous boundary layer permeability
P_p	passive permeability
S	substrate concentration
ACN	acetonitrile
LC/MS	liquid chromatography/ mass spectrometry
SIF	simulated intestinal fluid with pancreatic enzymes
CGH	choloylglycine hydrolase
DPBS	Dulbecco's phosphate buffered saline
PMSF	phenylmethylsulfonyl fluoride
EDTA	ethylenediaminetetraacetic acid
PEG	polyethylene glycol
RF	radiofrequency
FLASH	fast low angle shot
na	number of average
H&E	hematoxylin and eosin
FGF19	fibroblast growth factor 19

REFERENCES

1. Kullak-Ublick GA, Stieger B, Hagenbuch B, Meier PJ. Hepatic transport of bile salts. Semin Liver Dis. 2000; 20:273–292. [PubMed: 11076396]
2. Hofmann AF, Molino G, Milanese M, Belforter G. Description and simulation of a physiological pharmacokinetic model for the metabolism and enterohepatic circulation of bile acids in man. Cholic acid in healthy man. J Clin Invest. 1983; 71:1003–1022. [PubMed: 6682120]
3. Dawson, PA. Role of the intestinal bile acid transporters in bile acid and drug disposition.. In: Fromm, MF.; Kim, RB., editors. Handbook of experimental pharmacology. Vol. 201. Springer; New York: 2011. p. 169-203.
4. Montagnani M, Love MW, Rossel P, Dawson PA, Qvist P. Absence of dysfunctional ileal sodium-bile acid cotransporter gene mutations in patients with adult-onset idiopathic bile acid malabsorption. Scand J Gastroenterol. 2001; 36:1077–1080. [PubMed: 11589382]
5. Oelkers P, Kirby LC, Heubi JE, Dawson PA. Primary bile acid malabsorption caused by mutations in the ileal sodium-dependent bile acid transporter gene (SCL10A2). J Clin Invest. 1997; 99:1880–1887. [PubMed: 9109432]
6. Dawson PA, Haywood J, Craddock AL, Wilson M, Tietjen M, Kluckman K, Maeda N, Parks JS. Targeted deletion of the ileal bile acid transporter eliminates enterohepatic cycling of bile acids in mice. J Biol Chem. 2003; 278:33920–33927. [PubMed: 12819193]
7. Hofmann AF, Mangelsdorf DJ, Kliewer SA. Chronic diarrhea due to excessive bile acid synthesis and not defective ileal transport: A new syndrome of defective FGF19 release. Clin Gastroenterol Hepatol. 2009; 7:1151–1154. [PubMed: 19665580]
8. Smith MJ, Cherian P, Ruju GS, Dawson BF, Mahon S, Bardhan KD. Bile acid malabsorption in persistent diarrhoea. J R Coll Physicians Lond. 2000; 34:448–451. [PubMed: 11077656]
9. Williams AJ, Merrick MV, Eastwood MA. Idiopathic bile acid malabsorption—a review of clinical presentation, diagnosis, and response to treatment. Gut. 1991; 32:1004–1006. [PubMed: 1916479]
10. Merrick MV, Eastwood MA, Anderson JR, Ross HM. Enterohepatic circulation in man of a gamma-emitting bile-acid conjugate, 23-Selena-25-Homotaurocholic Acid (SeHCAT). J Nucl Med. 1981; 23:126–130. [PubMed: 7057253]

11. Yu JX, Kodibagkar VD, Cui W, Mason RP. 19F: A Versatile Reporter for Non-Invasive Physiology and Pharmacology Using Magnetic Resonance. Curr Med Chem. 2005; 12:819–848. [PubMed: 15853714]
12. Jiang ZX, Liu X, Jeong EK, Yu YB. Symmetry-guided design and fluorous synthesis of a stable and rapidly excreted imaging tracer for (19)F MRI. Angew Chem Int Ed Engl. 2009; 48:4755–4758. [PubMed: 19475598]
13. Raufman JP, Xu S, Cheng K, Khurana S, Johnson D, Shao C, Kane M, Shi D, Gullapalli R, Polli JE. In Vivo Magnetic Resonance Imaging to Detect Biliary Excretion of 19F-Labeled Drug in Mice. Drug Metab Dispos. 2011; 39:736–739. [PubMed: 21270105]
14. Vertzoni M, Archontaki H, Reppas C. Determination of intralumenal individual bile acids by HPLC with charged aerosol detection. J Lipid Res. 2008; 49:2690–2695. [PubMed: 18693215]
15. Balakrishnan A, Sussman DJ, Polli JE. Development of stably transfected monolayer overexpressing the human apical sodium-dependent bile acid transporter (hASBT). Pharm Res. 2005; 22:1269–1280. [PubMed: 16078136]
16. Leonhardt M, Keiser M, Oswald S, Kühn J, Jia J, Grube M, Kroemer HK, Siegmund W, Weitschies W. Hepatic uptake of the magnetic resonance imaging contrast agent Gd-EOB-DTPA: role of human organic anion transporters. Drug Metab Dispos. 2010; 38:1024–1028. [PubMed: 20406852]
17. Rais R, Gonzalez PM, Zheng X, Wring SA, Polli JE. Method to screen substrates of apical sodium-dependent bile acid transporter. AAPS J. 2008; 10:596–605. [PubMed: 19085111]
18. Balakrishnan A, Wring SA, Polli JE. Interaction of native bile acids with human apical sodium-dependent bile acid transporter (hASBT): Influence of steroidal hydroxylation pattern and C-24 conjugation. Pharm Res. 2006; 23:1451–1459. [PubMed: 16783481]
19. Balakrishnan A, Hussainzada N, Gonzalez P, Bermejo M, Swaan PW, Polli JE. Bias in estimation of transporter kinetic parameters from overexpression systems: Interplay of transporter expression level and substrate affinity. J Pharmacol Exp Ther. 2007; 320:133–144. [PubMed: 17038509]
20. Rais R, Fletcher S, Polli JE. Synthesis and *in vitro* evaluation of gabapentin prodrugs that target the human apical sodium-dependent bile acid transporter (hASBT). J Pharm Sci. 2010; 100:1184–1195. [PubMed: 20848648]
21. Vertzoni M, Fotaki N, Kostewicz E, Stippler E, Leuner C, Nicolaides E, Dressman J, Reppas C. Dissolution media simulating the intralumenal composition of the small intestine: physiological issues and practical aspects. J Pharm Pharmacol. 2004; 56:453–462. [PubMed: 15099440]
22. Huijghebaert SM, Hofmann AF. Influence of the amino acid moiety on deconjugation of bile acid amidates by cholylglycine hydrolase or human fecal cultures. J Lipid Res. 1986; 27:742–752. [PubMed: 2876046]
23. Frahm J, Haase A, Matthaei D. Rapid NMR imaging of dynamic processes using the FLASII technique. Magn Reson Med. 1986; 3:321–327. [PubMed: 3713496]
24. Haase A, Frahm J, Matthaei D, Haenicke W, Merboldt KD. FLASH imaging. Rapid NMR imaging using low flip-angle pulses. J Magn Reson. 1986; 67:258–266.
25. Committee for the Update of the Guide for the Care and Use of Laboratory Animals. National Research Council. Guide for the Care and Use of Laboratory Animals. 8th ed.. National Academies Press; Washington DC: 2011.
26. Kolhatkar V, Polli JE. Structural requirements of bile acid transporters: C-3 and C-7 modifications of steroidal hydroxyl groups. Eur J Pharm Sci. 2012; 46:86–99. [PubMed: 22387310]
27. Thomas C, Pellicciari R, Pruzanski M, Auwerx J, Schoonjans K. Targeting bile-acid signalling for metabolic diseases. Nat Rev Drug Discov. 2008; 7:678–693. [PubMed: 18670431]
28. Nguyen A, Bouscarel B. Bile acids and signal transduction: role in glucose homeostasis. Cell Signal. 2008; 20:2180–2197. [PubMed: 18634871]
29. Chiang JY. Bile acids: regulation of synthesis. J Lipid Res. 2009; 50:1955–1966. [PubMed: 19346330]
30. Houten SM, Watanabe M, Auwerx J. Endocrine functions of bile acids. Embo J. 2006; 25:1419–1425. [PubMed: 16541101]
31. Amaral JD, Viana RJ, Ramalho RM, Steer CJ, Rodrigues CM. Bile acids: regulation of apoptosis by ursodeoxycholic acid. J Lipid Res. 2009; 50:1721–34. [PubMed: 19417220]

32. Pedersen L, Arnfred T, Thaysen EH. Rapid screening of increased bile acid deconjugation and bile acid malabsorption by means of the glycine-l-(14 C) cholylglycine assay. Scand J Gastroenterol. 1973; 8:665–672. [PubMed: 4768311]
33. Brydon WG, Nyhlin H, Eastwood MA, Merrick MV. Serum 7 alpha-hydroxy-4-cholesten-3-one and selenohomocholyltaurine (SeHCAT) whole body retention in the assessment of bile acid induced diarrhoea. Eur J Gastroenterol Hepatol. 1996; 8:117–23. [PubMed: 8723414]
34. Lenicek M, Duricova D, Komarek V, Gabrysova B, Lukas M, Smerhovsky Z, Vitek L. Bile acid malabsorption in inflammatory bowel disease: Assessment by serum markers. Inflamm Bowel Dis. 2011; 17:1322–1327. [PubMed: 21058331]
35. Khalid U, Lalji A, Stafferton R, Andreyev J. Bile acid malabsorption: a forgotten diagnosis? Clin Med. 2010; 10:124–126. [PubMed: 20437979]
36. Wedlake L, Thomas K, Lalji A, Anagnostopoulos C, Andreyev HJ. Effectiveness and tolerability of colesevelam hydrochloride for bile-acid malabsorption in patients with cancer: a retrospective chart review and patient questionnaire. Clin Ther. 2009; 31:2549–2558. [PubMed: 20109999]
37. Zheng X, Ekins S, Raufman JP, Polli JE. Computational models for drug inhibition of the human apical sodium-dependent bile acid transporter. Mol Pharm. 2009; 6:1591–1603. [PubMed: 19673539]
38. Salvioli G, Lugli R, Pradelli JM, Gigliotti G. Bile acid binding in plasma: the importance of lipoproteins. FEBS Lett. 1985; 187:272–276. [PubMed: 4018265]
39. Ruiz-Cabello J, Barnett BP, Bottomley PA, Bulte JW. Fluorine (^{19}F) MRS and MRI in biomedicine. NMR Biomed. 2011; 24:114–129. [PubMed: 20842758]
40. Rais R, Acharya C, MacKerell AD Jr. Polli JE. Structural determinants for transport across the intestinal bile acid transporter using C-24 bile acid conjugates. Mol Pharm. 2010; 7:2240–2254. [PubMed: 20939504]

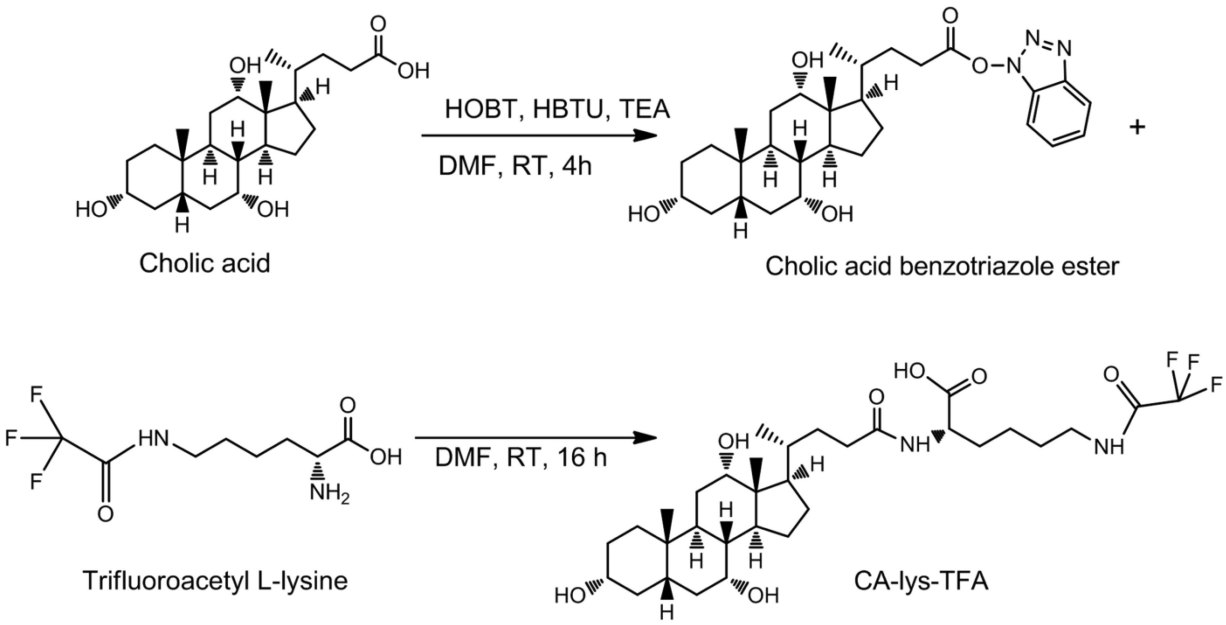

Figure 1.
Cholic acid-trifluoroacetyl lysine (CA-lys-TFA) synthesis. Cholic acid was first activated by formation of an OBt ester, then conjugated to trifluoroacetyl L-lysine.

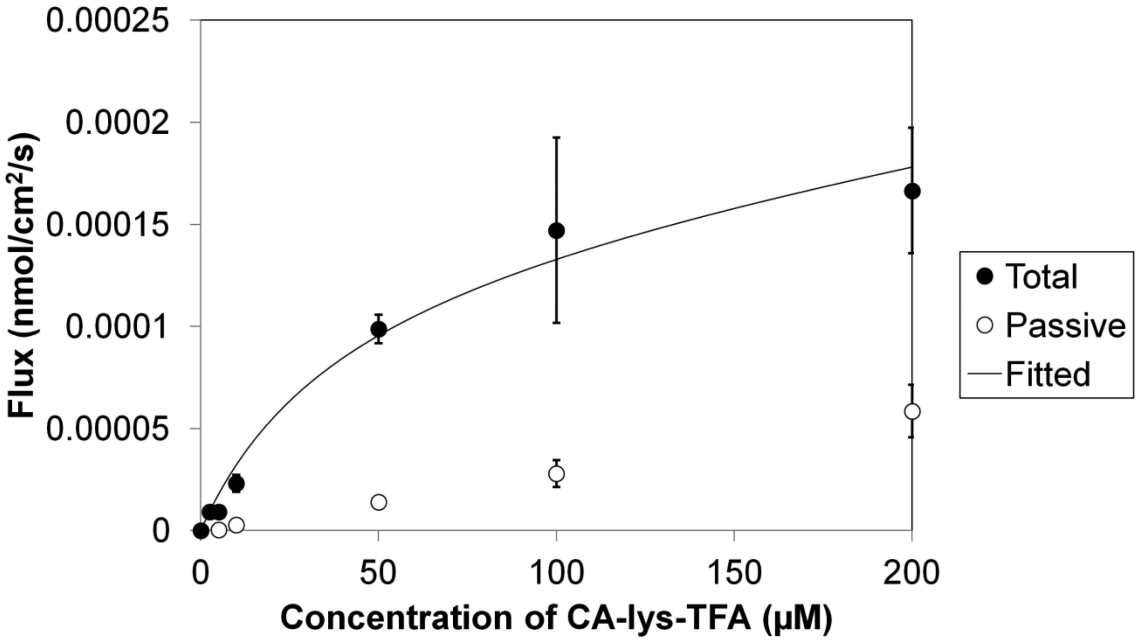

Figure 2.
Uptake of CA-lys-TFA by hASBT. Total uptake flux was obtained using HBSS. Passive flux was obtained using SFB. At 10 μM, total uptake was 8.01 times that of passive uptake.

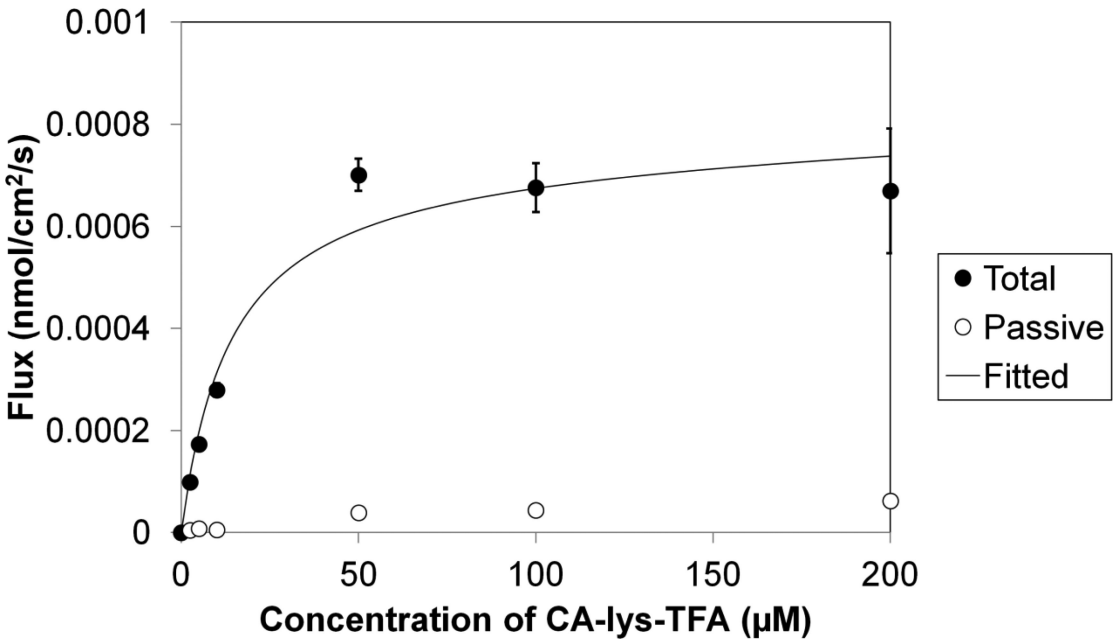

Figure 3.
Uptake of CA-lys-TFA by hNTCP. Total uptake flux was obtained using HBSS (Hank's Balanced Salt Solution). Passive flux was obtained using sodium free buffer (SFB). At 10 μM, total uptake was 49.6 times that of passive uptake.

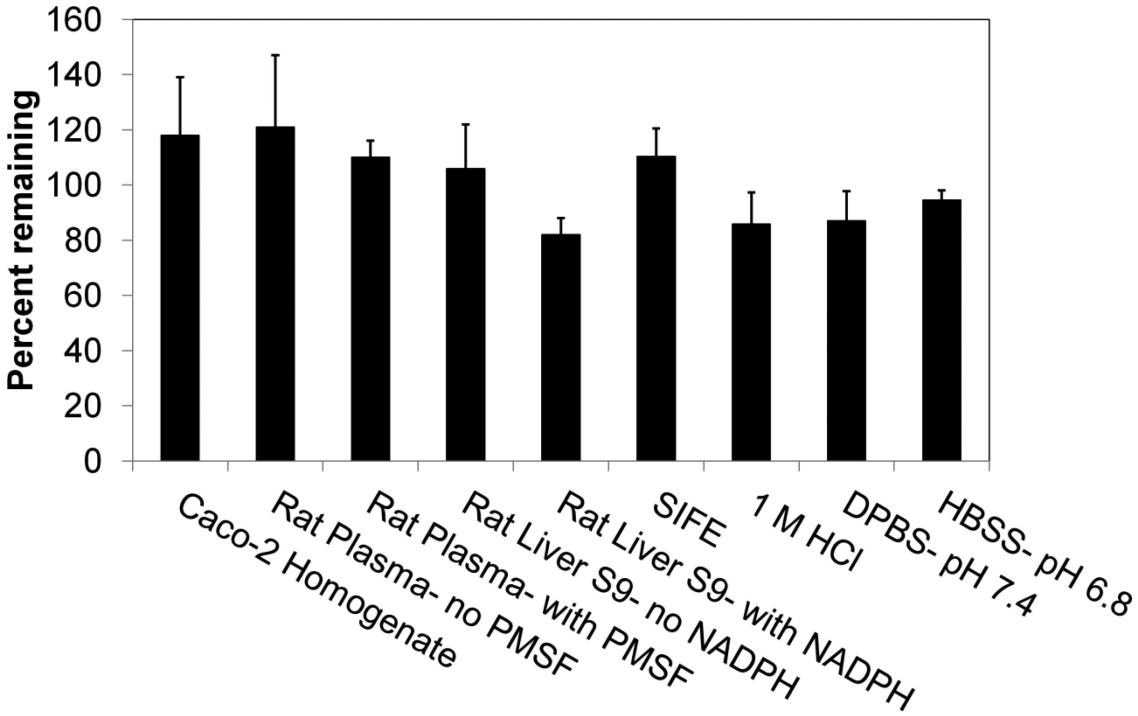

Figure 4.

Stability of CA-lys-TFA under nine conditions. The nine conditions were Caco-2 homogenate, rat plasma with and without PMSF (phenylmethylsulfonyl fluoride), rat liver S9 fraction with and without NADPH, SIF (simulated intestinal fluid with pancreatic enzymes), 1 M HCl, and buffer at pH 7.4 and pH 6.8. Stability study duration was 4 h, except DPBS and HBSS used 3 h. The percent remaining did not different from initial amount ($p>0.097$; Student's paired *t*-test). Each study was performed in triplicate.

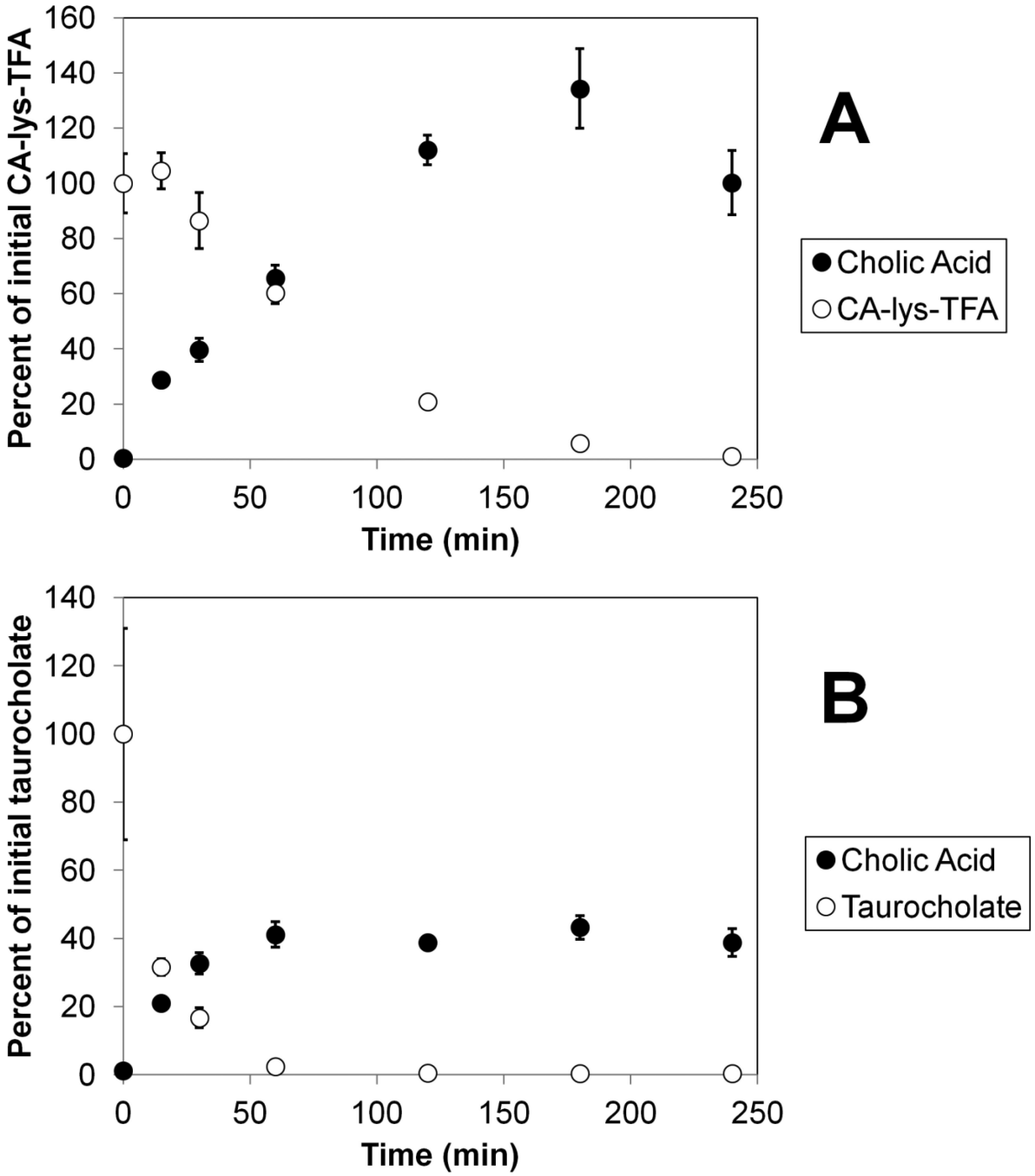

Figure 5.

Comparative stabilities of CA-lys-TFA and taurocholate against choloylglycine hydrolase from *Clostridium perfringens*. Panel A shows the loss of CA-lys-TFA (initially 2 mM) and the corresponding appearance of deconjugated cholic acid. Panel B shows the loss of taurocholate (initially 2 mM) and the corresponding appearance of deconjugated cholic acid. Each study was performed in triplicate. After 1 h, only 2.4% of taurocholate remained, while 60.4% of CA-lys-TFA remained, suggesting improved stability of the amide bond linking trifluoroacetyl lysine to cholic acid, compared to the natural amino acid conjugate.

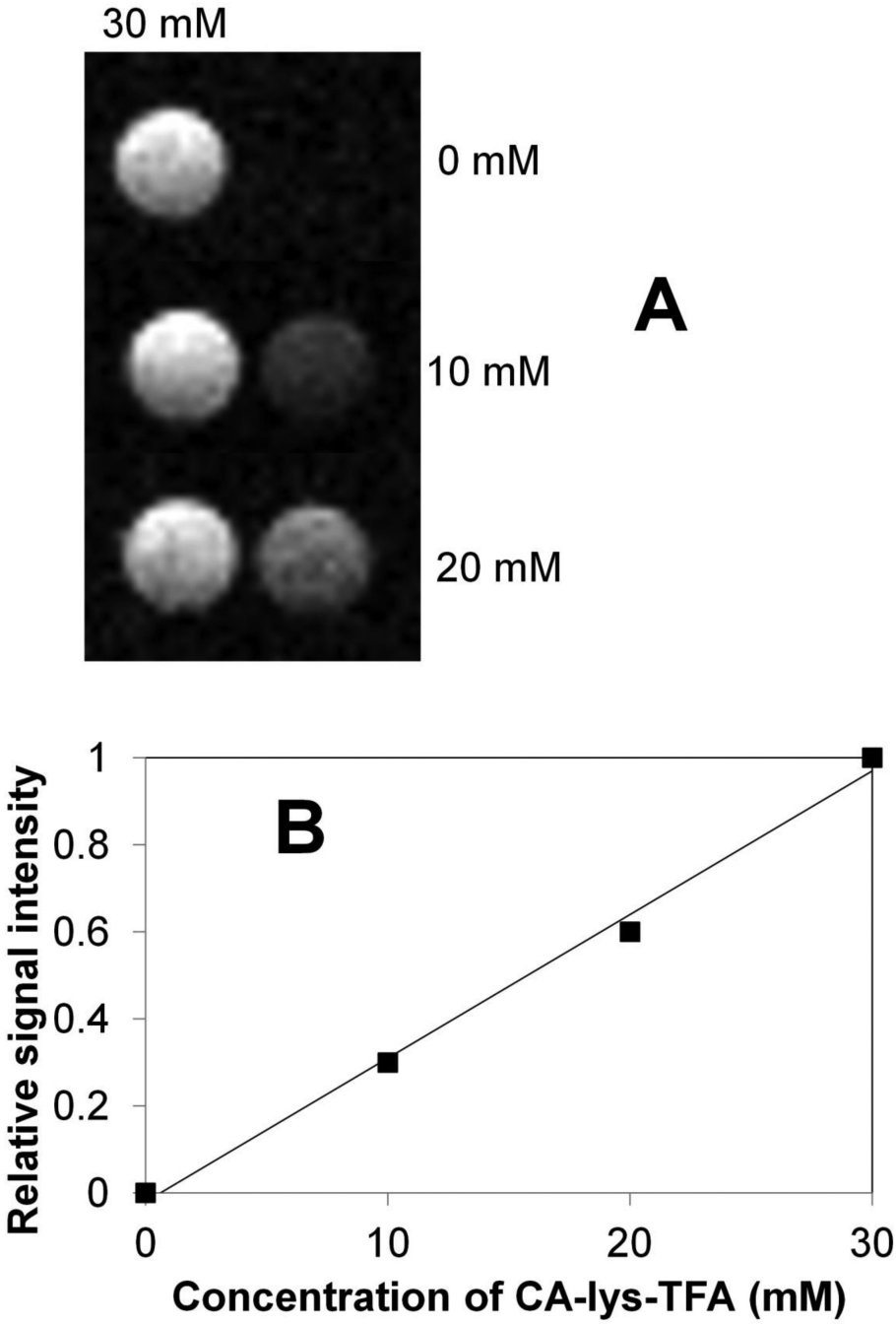

Figure 6.

In vitro ^{19}F MRI images of 0, 10, and 20 mM CA-lys-TFA alongside a 30 mM CA-lys-TFA vial for each sample (panel A) and their corresponding signal intensities relative to the 30-mM vial (panel B). Signal intensities were found to linearly correspond to concentration. The line was obtained from linear regression.

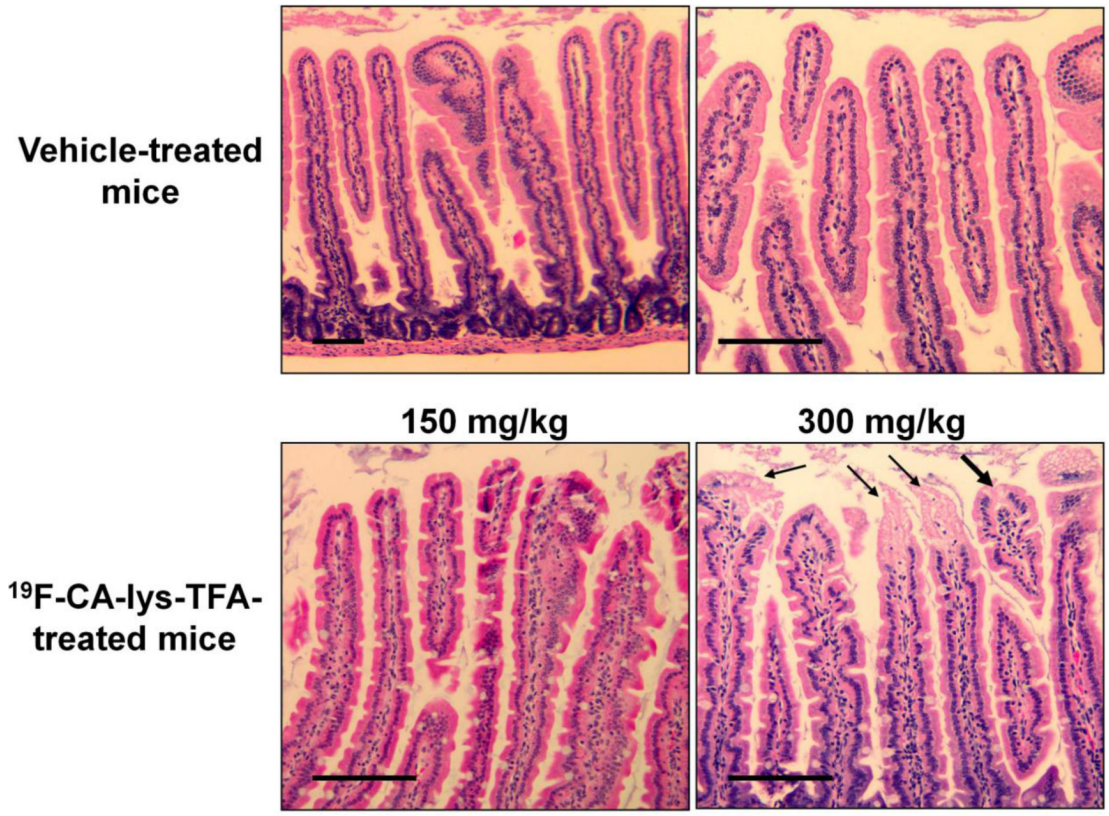

Figure 7.

Representative microscopic images of H&E-stained intestinal villi following treatment with vehicle or two doses of CA-lys-TFA. Intestinal villi from vehicle- and low-dose (150 mg/kg) CA-lys-TFA -treated mice show intact surface epithelium at the tips of small intestinal villi. In contrast, in two of three mice treated with high-dose (300 mg/kg) CA-lys-TFA cellular injury at the tips of intestinal villi was observed (lower, right panel). Villus injury in mice treated with high-dose CA-lys-TFA is characterized by loss of nuclei and cytoplasmic vacuolization in a few cells (thick arrow). Confluent necrosis of the epithelial tip lining with early sloughing toward the lumen is noted in adjacent villi marked with thin arrows. Size bars = 100 micrometers.

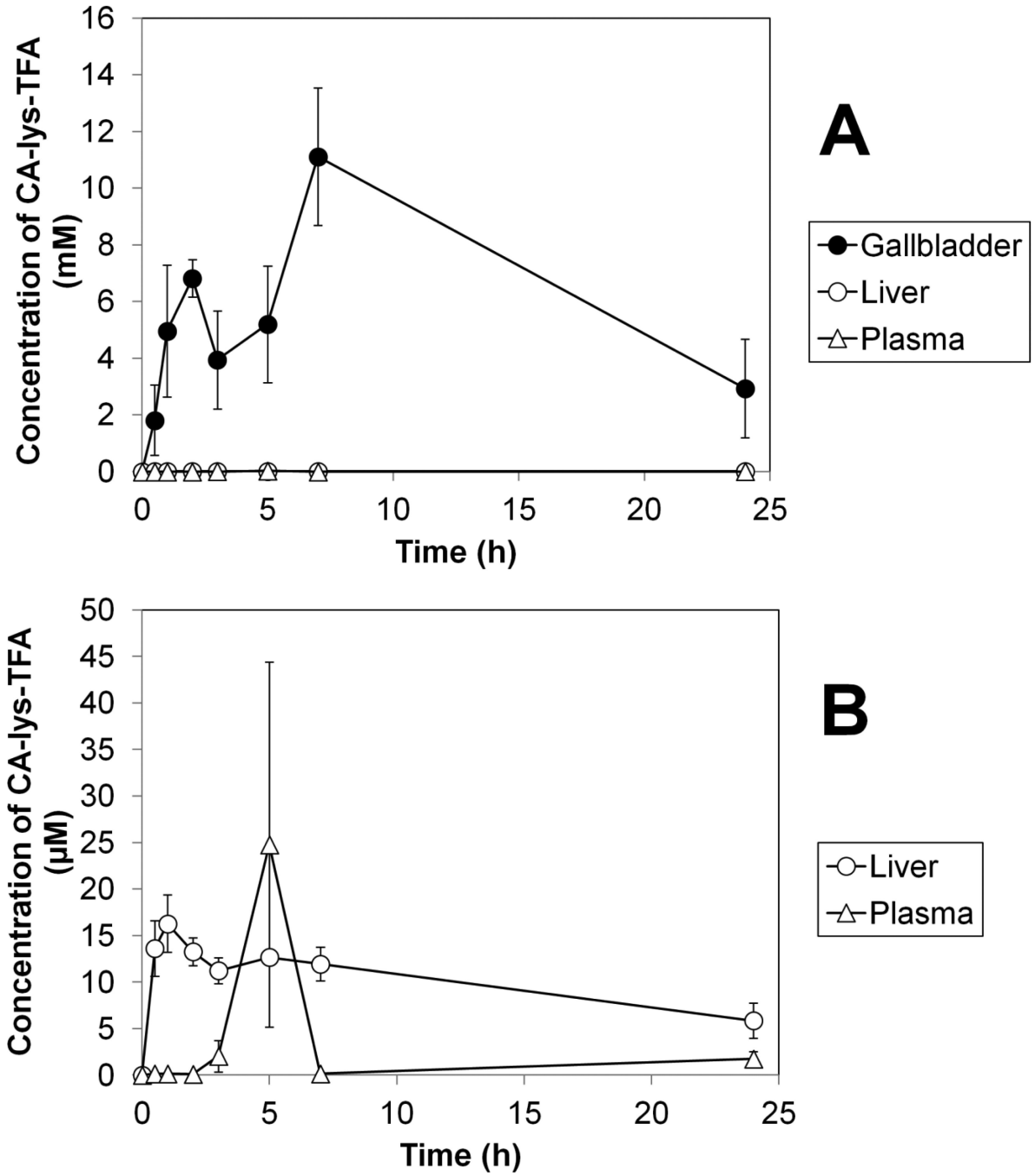

Figure 8.

Average concentration versus time of CA-lys-TFA after oral administration of 50 mg/kg CA-lys-TFA. Panel A shows CA-lys-TFA concentration in gallbladder, liver, and plasma. CA-lys-TFA in gallbladder was generally over 500-fold higher than in liver or plasma. Panel B slows an expanded plot, to better visualize the lower concentrations in liver and plasma.

Table I

Summary of *in vivo* CA-lys-TFA disposition into the gallbladder, liver, and plasma. Three doses of CA-lys-TFA were studied (0, 150, and 300 mg/kg). For the 150 and 300 mg/kg doses, at least 21.0 μmol compound/g gallbladder was present in the gallbladder at t = 5 h.

	Dose CA-lys-TFA (mg/kg)		
	0	**150**	**300**
Gallbladder weight (mg)	14.4 ± 4.8	25.2 ± 3.2	17.1 ± 4.9
Gallbladder concentration (mM)	0	27.0 ± 2.4	36.8 ± 8.8
Percent of dose in gallbladder	0	11.0 ± 1.7	5.33 ± 1.98
Liver concentration (mM)	0	0.0788 ± 0.0351	0.0571 ± 0.0104
Plasma concentration (μM)	0	0.444 ± 0.169	0.418 ± 0.015

Table II

Non-compartmental pharmacokinetic parameters of CA-lys-TFA after oral administration of 50 mg/kg.

	C_{max} (mM)	T_{max} (h)	AUC $_{0\rightarrow 24h}$ (mM*h)
Plasma	0.0248 ± 0.0196	5	0.0540
Liver	0.0163 ± 0.0031	1	0.232
Gall Bladder	11.1 ± 2.4	7	143